

New empirical constraints on the cosmological evolution of gas and stars in galaxies

Hamsa Padmanabhan^{1*} and Abraham Loeb^{2†}

¹ Canadian Institute for Theoretical Astrophysics, 60 St. George Street, Toronto, ON M5S 3H8, Canada

² Astronomy department, Harvard University, 60 Garden Street, Cambridge, MA 02138, USA

Accepted —. Received —; in original form —

ABSTRACT

We combine the latest observationally motivated constraints on stellar properties in dark matter haloes, along with data-driven predictions for the atomic (HI) and molecular (H₂) gas evolution in galaxies, to derive empirical relationships between the build-up of galactic components and their evolution over cosmic time. At high redshift ($z \gtrsim 4$), the frameworks imply that galaxies acquire their cold gas (both atomic and molecular) mostly by accretion, with the fraction of cold gas reaching about 20% of the cosmic baryon fraction. We infer a strong dependence of the star formation rate on the H₂ mass, suggesting a near-universal depletion timescale of 0.1–1 Gyr in Milky Way sized haloes (of masses $10^{12} M_{\odot}$ at $z = 0$). There is also evidence for a near-universality of the Kennicutt-Schmidt relation across redshifts, with very little dependence on stellar mass, if a constant conversion factor (α_{CO}) of CO luminosity to molecular gas mass is assumed. Combining the atomic and molecular gas observations with the stellar build-up illustrates that galactic mass assembly in Milky-Way sized haloes proceeds from smooth accretion at high redshifts, towards becoming merger-dominated at late times ($z \lesssim 0.6$). Our results can be used to constrain numerical simulations of the dominant growth and accretion processes of galaxies over cosmic history.

Key words: galaxies: star formation - galaxies: evolution - galaxies: high-redshift

1 INTRODUCTION

The so-called ‘baryon cycle’ in galaxies offers novel insights into the inter-relationship between gas and stellar evolution across cosmic time. While we do not yet have a complete picture of the details of galaxy formation (for a review, see, e.g., Naab & Ostriker (2017)), some of the outstanding questions include: (i) the relative contributions of mergers and smooth accretion to the gas assembly in galaxies (e.g., Kereš et al. 2005; Dekel et al. 2009; Nelson et al. 2013), as a function of halo mass and cosmic time, (ii) whether the physical processes governing star formation at high redshifts differ from those in the local universe, and (iii) the precise roles of atomic (HI) and molecular (H₂) gas (e.g., Daddi et al. 2010a; Tacconi et al. 2013; Saintonge et al. 2017) in driving the cosmological star formation rate.

Various semi-analytical and simulation methods have been used to predict the cosmological evolution of gas and stars in galaxies. While Semi-Analytical Methods (SAMs; e.g. Guo et al. 2010; Benson 2012; Somerville et al. 2008; Popping et al. 2014; Somerville & Davé 2015) use sophisticated prescriptions having free parameters to model the physical parameters associated with the gas, stellar, black hole and radiation associated with galax-

ies, detailed hydrodynamical codes (e.g., Naab & Ostriker 2017; Tacchella et al. 2019) explicitly simulate these processes in a cosmological setting. Analytical techniques, such as toy models (e.g., Bouché et al. 2010; Dekel et al. 2013; Lilly et al. 2013) offer a complementary sketch for the stellar and gas build-up.

An alternative approach to constrain galaxy evolution is the empirical (data-driven) framework, in which observationally measured quantities are used to set direct constraints on the properties of gas and stars in haloes. For the Λ CDM cosmological scenario, several empirical studies have placed constraints on the stellar properties in galaxies across cosmic time (e.g., Behroozi et al. 2013c; Moster et al. 2013; Girelli et al. 2020; Tacchella et al. 2018; Rodríguez-Puebla et al. 2017; Behroozi et al. 2019) such as the stellar mass - halo mass (SHM) relation, using the technique of *abundance matching*. Such methods have been extended to atomic and molecular gas in Popping et al. (2015) by using physical prescriptions connecting gas profiles and stellar masses of galaxies. For atomic gas (HI) in galaxies, Padmanabhan et al. (2017) used the combination of presently available data from galaxy surveys, HI intensity mapping experiments and Damped Lyman Alpha (DLA) observations to constrain an empirical HI mass - halo mass relation (HIHM). The inferred HIHM was found to be characterized by three free parameters and does not evolve strongly with redshift. In Padmanabhan & Kulkarni (2017), an equivalent, local HIHM was derived by matching the abundances of HI galaxies (at $z \sim 0$)

* Email: hamsa@cita.utoronto.ca

† Email: aloeb@cfa.harvard.edu

observed in the HIPASS survey (Zwaan et al. 2005a) to the mass function of dark matter haloes (Sheth & Tormen 2002).¹

The primary observational tracer of molecular gas (H_2) is carbon monoxide (CO) which is strongly connected to the star formation rate. In Padmanabhan (2018), constraints on the CO luminosity function at low redshifts (Keres et al. 2003) were combined with intensity mapping observations at $z \sim 3$ from the CO Power Spectrum Survey (COPSS; Keating et al. 2016) to predict the evolution of the CO luminosity - halo mass ($L_{CO} - M$) relation via abundance matching. The observations were found to be consistent with a well-defined $L_{CO} - M$ having four free parameters, motivated by the empirical SHM of Moster et al. (2013). In contrast to the HIHM, the inferred $L_{CO} - M$ is observed to show a significant evolution across $z \sim 0 - 4$.

The extended Press-Schechter (EPS) formalism provides a convenient framework to compute the assembly history of a given dark matter halo via mergers of smaller haloes (Sheth & Tormen 2002). Merger trees computed from numerical simulations (e.g., Klypin et al. 2011) allow the tracking of the most massive (main) progenitor halo for a given halo across cosmic time. In this paper, we combine the empirically determined prescriptions connecting the stellar (Behroozi et al. 2013c, 2019), atomic (Padmanabhan et al. 2017) and molecular (Padmanabhan 2018) gas in galaxies to haloes, with the merger tree framework that describes halo assembly, to provide an understanding of the growth histories of the various galactic components and their dependences on each other. This analysis extends previous work to construct ‘baryon progenitor trees’ which are directly motivated by observations. In so doing, it sheds light into the relative contributions of mergers and smooth accretion to gas mass assembly, and the dependence of the star formation history on the atomic and molecular gas depletion timescales.² Being completely empirical, this study is free from the uncertainties involved in physical models of stellar and gas evolution in galaxies. As such, it provides an important benchmark for calibrating the detailed physics in current and forthcoming simulations of galaxy formation, and enables the understanding of the dominant processes involved therein.

The outline of this paper is as follows. In Sec. 2, we present the formalism which associates gas to dark matter haloes, which we connect to the empirical framework for the evolution of the stellar component in Sec. 3. Finally, Sec. 4 summarizes our main results.

2 HALO MODEL FRAMEWORKS FOR ATOMIC AND MOLECULAR GAS

In this section, we briefly review the existing empirical frameworks developed for associating atomic and molecular gas to dark matter haloes. For atomic gas (HI), we use the halo model for cosmological neutral hydrogen (Padmanabhan et al. 2017), which combines constraints from HI galaxy surveys at $z \sim 0$ (Zwaan et al. 2005a,b;

Martin et al. 2010, 2012; Braun 2012), intensity mapping experiments (around $z \sim 1$; e.g. Switzer et al. 2013) and the statistics of Damped Lyman Alpha (DLA) systems (column density distributions, incidences and three dimensional clustering; Rao et al. 2006; Prochaska & Wolfe 2009; Noterdaeme et al. 2012; Font-Ribera et al. 2012; Zafar et al. 2013) across $z \sim 0 - 5$. The results of a joint fit to all these datasets favour a well-defined mean HI mass - halo mass relation:

$$M_{HI}(M, z) = \alpha_{HI} f_{H,c} M \left(\frac{M}{10^{11} h^{-1} M_{\odot}} \right)^{\beta} \times \exp \left[- \left(\frac{v_{c0}}{v_c(M, z)} \right)^3 \right], \quad (1)$$

with the three parameters (i) $\alpha_{HI} = 0.09 \pm 0.01$, which denotes the average HI fraction relative to cosmic $f_{H,c}$, (ii) $\beta = -0.58 \pm 0.06$, the logarithmic slope of the relation which represents the deviation from linearity of the prescription, and (iii) v_{c0} , given by $\log(v_{c0}/\text{km s}^{-1}) = 1.58 \pm 0.04$ which denotes the minimum virial velocity below which haloes preferentially do not host HI. The halo mass function used for this purpose is that of Sheth & Tormen (2002).

To describe the molecular gas (H_2) evolution, we use the results of Padmanabhan (2018), which infers a CO luminosity - halo mass relation having the physically motivated form:

$$L_{CO}(M, z) = 2N(z)M[(M/M_1(z))^{-b(z)} + (M/M_1(z))^{y(z)}]^{-1}, \quad (2)$$

with the parameters $M_1(z)$, $N(z)$, $b(z)$ and $y(z)$ themselves consisting of two terms - a constant term which describes the behaviour at $z \sim 0$, and an evolutionary component:

$$\begin{aligned} \log M_1(z) &= \log M_{10} + M_{11}z/(z+1); \\ N(z) &= N_{10} + N_{11}z/(z+1); \\ b(z) &= b_{10} + b_{11}z/(z+1); \\ y(z) &= y_{10} + y_{11}z/(z+1). \end{aligned} \quad (3)$$

The best fitting values for these parameters, found from fitting the observations of Keres et al. (2003) at $z \sim 0$ are given by $M_{10} = (4.17 \pm 2.03) \times 10^{12} M_{\odot}$, $N_{10} = 0.0033 \pm 0.0016 \text{ K km/s pc}^2 M_{\odot}^{-1}$, $b_{10} = 0.95 \pm 0.46$, $y_{10} = 0.66 \pm 0.32$. The evolutionary components, derived by subsequently matching the COPSS results (Keating et al. 2016) at $z \sim 3$ are given by:

$$\begin{aligned} M_{11} &= -1.17 \pm 0.85; \\ N_{11} &= 0.04 \pm 0.03; \\ b_{11} &= 0.48 \pm 0.35; \\ y_{11} &= -0.33 \pm 0.24. \end{aligned} \quad (4)$$

The above framework can be converted into an equivalent H_2 mass to halo mass evolution by assuming a CO luminosity - H_2 mass conversion factor. The value of this factor – denoted by α_{CO} , and defined through $M_{H_2} = \alpha_{CO} L_{CO}$ (with M_{H_2} in units of M_{\odot} and L_{CO} in units of K km/s pc^2) – and its evolution are still observationally uncertain. Several studies (e.g., Bolatto et al. 2013) advocate the present value of α_{CO} to be of order unity, and recent ALMA evidence (e.g. Cortese et al. 2017) indicating a higher fraction of molecular gas at high redshifts compared to atomic, may be consistent with a non-varying α_{CO} . Throughout this work, we assume $\alpha_{CO} = 0.8$ across all redshifts under consideration.³

³ A decreasing trend of α_{CO} with z may be advocated by the observational

¹ Combining the HIHM so derived with the SHM obtained by Moster et al. (2013) led to an inferred HI-stellar evolution which was consistent with various $z = 0$ measurements: from the Galex Arecibo SDSS Survey (GASS; Catinella et al. 2010, 2013), COLD GASS (Saintonge et al. 2011b,a; Catinella et al. 2012), the HERA CO Line Extragalactic Survey (HERACLES; Leroy et al. 2009) and The HI Nearby Galaxy Survey (THINGS; Walter et al. 2008).

² Assembly bias and environmental effects are expected to have a small to negligible effect on the halo models for baryonic gas, whose spatial extents are much smaller than the dark matter virial radius.

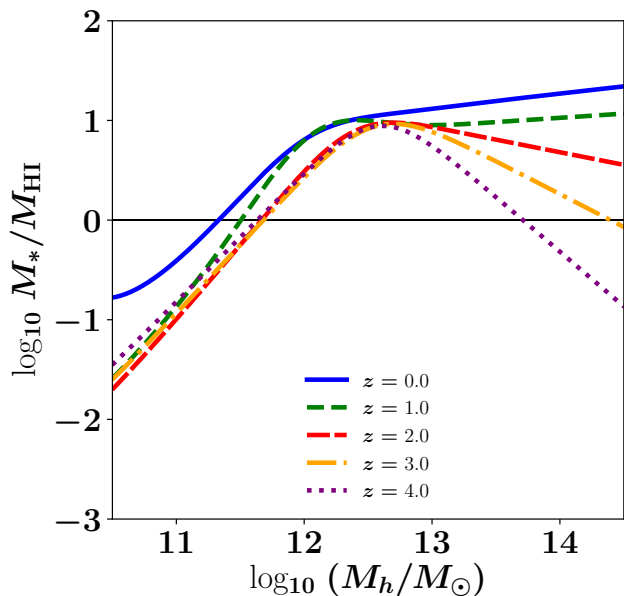


Figure 1. Ratio of the average stellar mass $M_*(M_h, z)$ predicted by the SHM relation of Behroozi et al. (2019) to the average HI mass, $M_{\text{HI}}(M_h, z)$ predicted from the HIHM of Padmanabhan et al. (2017) in host dark matter haloes as a function of their halo masses M_h , for different redshifts $z = 0$ to 4. A ratio of unity (equal stellar and HI masses) is indicated by the black solid line.

3 BUILD-UP OF GAS AND STELLAR COMPONENTS

3.1 Evolution of dark matter and stellar components

We can now combine the gas halo models outlined in Sec. 2 with the existing results linking stellar properties in galaxies with their host dark matter haloes. For dark matter, we use the halo masses and accretion histories from the compilation in Behroozi et al. (2013c), which are based on the *Bolshoi* simulations of Klypin et al. (2011) with haloes identified using the ROCKSTAR halo finder (Behroozi et al. 2013a) and the corresponding merger trees (Behroozi et al. 2013b). The *Bolshoi* results were supplemented by those from two larger simulations: Riebe et al. (*MultiDark*; 2011) and Behroozi et al. (Consuelo; 2013b) for accuracy and resolution purposes. The combined simulation dataset allows to construct the trajectory of the most massive progenitor halo at each redshift for a given descendant halo at $z = 0$.

For the stellar component, we use the results of Behroozi et al. (2019), who combine observational data collected from the Sloan Digital Sky Survey (SDSS), the PRISM Multi-object Survey (PRIMUS), UltraVISTA, the Cosmic Assembly Near-infrared Deep Extragalactic Legacy Survey (CANDELS), and the FourStar Galaxy Evolution Survey (ZFOURGE) over $0 < z < 10.5$ to derive empirical constraints on the stellar mass to halo mass relation across cosmic time. We also use the publicly available catalogs of empirically determined star formation histories from Behroozi et al. (2013c) (derived from a wide range of overlapping surveys

results of Carleton et al. (2017) - which find about a ~ 1 dex decline in α_{CO} between redshifts 0 and redshifts 3-4 (see also Bolatto et al. 2013). Since the detailed behaviour of α_{CO} with redshift is essentially unconstrained, we prefer to stick with a non-varying value of α_{CO} in the present work.

over $z = 0$ to 8) for the evolution of the star formation rate across redshifts.

3.2 Connecting gas and stellar evolution

We can now use the results of Sec. 2 with the empirically derived stellar-halo mass relations to study the gas-galaxy connection across cosmic time. We begin by combining the empirical HIHM of Padmanabhan et al. (2017) with the corresponding SHM derived by Behroozi et al. (2019) to plot the ratio of the stellar mass to the HI mass (M_*/M_{HI}) in galaxies, as a function of the host halo mass M_h and redshift z , in Fig. 1. The figure indicates that the ratio of HI to stellar mass is fairly independent of redshift and only depends on halo mass, up to halo masses of $M_h \sim 10^{13} M_\odot$.

It was found in Padmanabhan & Kulkarni (2017) that the local ($z \sim 0$) HI-mass to stellar-mass ratio is about 25% in the rather broad range of halo masses from 10^{11} to $10^{13} M_\odot$ and decreases to about 10% at halo masses above this range. The differences between the present results at $z = 0$ and those of Padmanabhan & Kulkarni (2017, see Fig. 2 of that paper) in the low halo mass regime stem from the slightly different methodologies and datasets used to calibrate the HI-halo mass (HIHM) and stellar mass-halo mass (SHM) relations in Padmanabhan & Kulkarni (2017), relative to those used here. Specifically, it is known that at $M_h \lesssim 10^{11} M_\odot$, abundance matching of HI gas in haloes from the HIPASS and ALFALFA datasets (Padmanabhan & Kulkarni 2017) predicts a somewhat lower (by ~ 1 dex) average HI mass fraction than a forward modelling MCMC-based approach to the HI observations at $z \sim 0 - 5$ (Padmanabhan et al. 2017). On the other hand, the analysis of Moster et al. (2013) used in Padmanabhan & Kulkarni (2017) predicts a somewhat larger stellar mass ratio relative to that in Behroozi et al. (2019) used here. The above two trends, taken together, lead to the observed differences between in the low halo mass regime, which are nevertheless within the scatter involved in the relevant SHM and HIHM relations (of the order of 10% to 20%). The SHM relation developed by other approaches, e.g. that of Rodríguez-Puebla et al. (2017) is also consistent with Behroozi et al. (2019) at all halo masses in the range considered here (as illustrated in Fig. 34 of Behroozi et al. (2019)), hence, using other SHM forms in the literature are also not expected to change the results significantly within the expected uncertainties.

3.3 Baryonic build-up: accretion and mergers

Combining the dark matter merger trees described in Sec. 3.1 and the empirical SHM relation (Behroozi et al. 2019) leads to the evolution of the stellar mass trajectories across cosmic time. Analogous trajectories for the gas mass build-up can now be constructed by populating the dark matter merger trees with the gas-halo mass connections described in Sec. 2. Both these sets of trajectories are shown in Figs. 2 as a function of cosmic age, for four descendant dark matter halo masses ($10^{11} M_\odot$, $10^{12} M_\odot$, $10^{13} M_\odot$, and $10^{14} M_\odot$) at $z = 0$. Each figure shows the ratio of the stellar ($M_*(z)$, blue dashed lines) and gas masses ($M_{\text{HI}}(z) + M_{\text{H}_2}(z)$, orange solid lines) to the progenitor halo mass $M_h(z)$, normalized to the cosmic baryon fraction $f_b = \Omega_b/\Omega_m$. The plots assume a constant value of $\alpha_{\text{CO}} = 0.8$ for converting CO luminosity to H_2 mass.

The figures show that the star formation efficiency is highest in haloes of masses $M_h(z = 0) \sim 10^{12} M_\odot$ today, with the stellar mass growing at the expense of the halo mass and reaching about

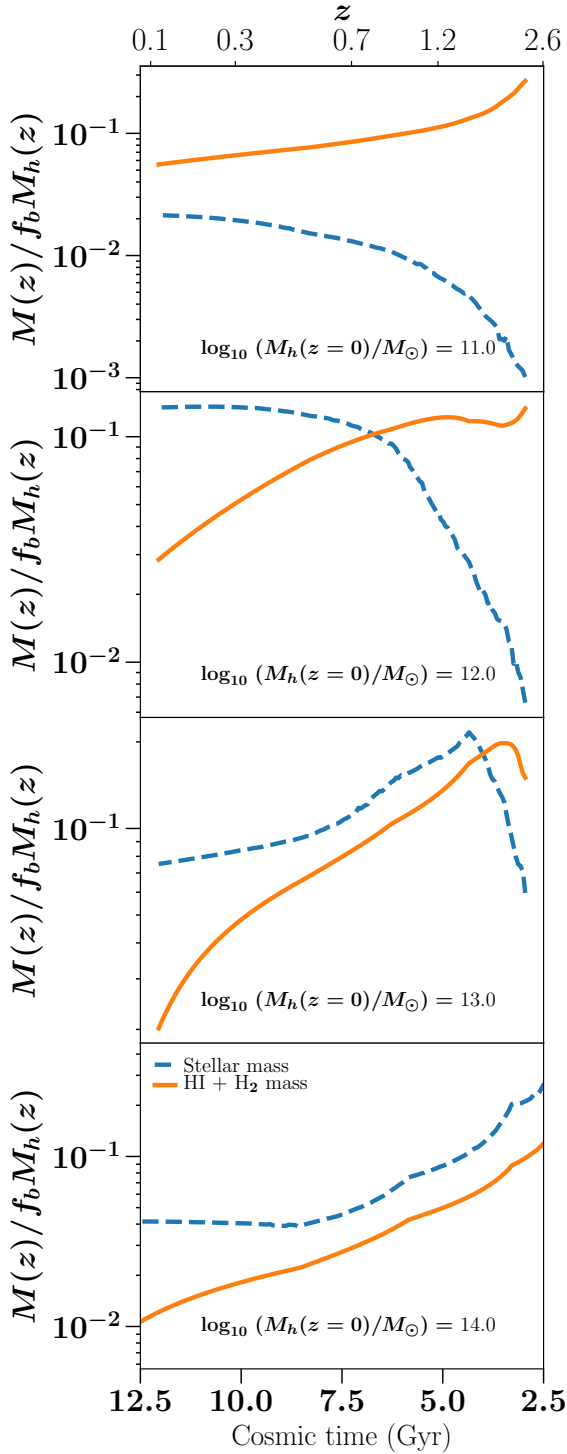


Figure 2. Evolution of the ratio of baryonic gas (HI + H₂; orange solid lines) mass and stellar (blue dashed lines) mass to the progenitor host halo mass, relative to the cosmological baryon fraction ($f_b = \Omega_b/\Omega_m$). The plots assume a constant value of $\alpha_{\text{CO}} = 0.8$ for converting CO luminosity to H₂ mass. From top to bottom, the panels show the evolution of these components with redshift z in the most massive progenitors of dark matter haloes having masses $M_h(z=0) = 10^{11}, 10^{12}, 10^{13}$ and $10^{14} M_\odot$ today.

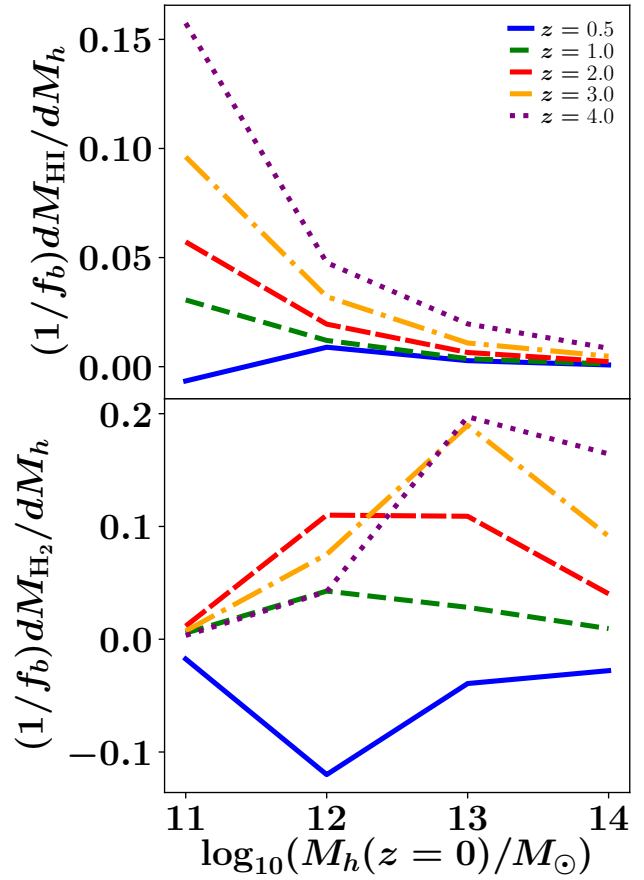


Figure 3. Ratio of the differential change in cold gas mass to that in host halo mass, dM_{HI}/dM_h (top panel) and dM_{H_2}/dM_h (lower panel) in the most massive progenitors of dark matter haloes, as a function of the descendant halo masses M_h at $z=0$. The ratios are indicated for redshifts $z = 0.5 - 4$ and normalized to the cosmic baryon fraction $f_b = \Omega_b/\Omega_m$. A constant value of $\alpha_{\text{CO}} = 0.8$ is assumed for converting CO luminosity to H₂ mass.

20% of the cosmic baryon fraction by $z \sim 0$. At lower halo masses ($\sim 10^{11} M_\odot$), the gas depletion and stellar build-up show the same trend but the curves are shallower, with the stellar and gas fractions reaching a few percent of the cosmic baryon fraction by $z \sim 0$. At higher halo masses, the baryonic conversion efficiency is lower and decreases with cosmic time, and the proportion of neutral gas is smaller at $z \sim 0$ than for $10^{12} M_\odot$ haloes. The stellar and gas fractions in haloes of masses $\sim 10^{13} - 10^{14} M_\odot$ today peaked around $z \sim 2$, and account for between a few and 10 percent of f_b by $z \sim 0$. These results are broadly consistent with those found in earlier semi-empirical studies: [Behroozi et al. \(2013c\)](#) and [Popping et al. \(2015\)](#), who use different prescriptions to connect atomic and molecular gas to stellar masses in galaxies.

The two main modes of gas assembly in galaxies are by smooth accretion from the intergalactic medium (IGM) and mergers. Insight into smooth gas accretion may be gained by measuring what fraction of the baryon inflow turns into the atomic and molecular gas (HI and H₂) of the central galaxy. This is quantified in the panels of Fig. 3, which plot the ratios of the differential baryonic gas mass ($dM_{\text{HI}}, dM_{\text{H}_2}$) to the differential halo mass (dM_h), normalized to the cosmic baryon fraction f_b . The differential mass

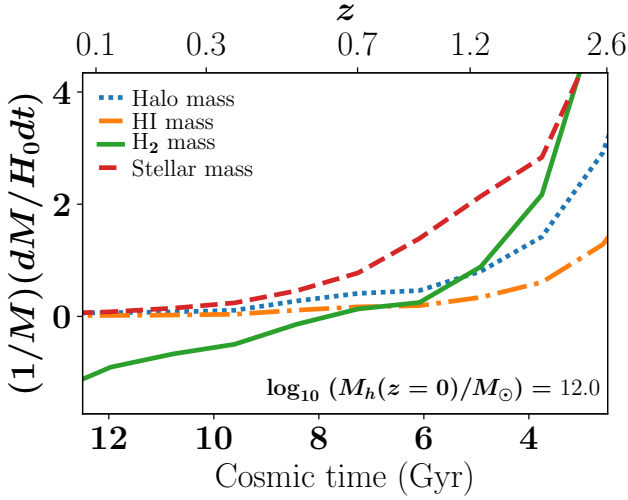


Figure 4. Logarithmic derivatives of the progenitor halo ($dM_h/M_h H_0 dt$, blue dotted curve), HI ($dM_{\text{HI}}/M_{\text{HI}} H_0 dt$, orange dot-dashed curve), H_2 ($dM_{\text{H}_2}/M_{\text{H}_2} H_0 dt$, green solid curve) and stellar ($dM_*/M_* H_0 dt$, red dashed curve) masses with respect to time, in a fiducial descendant dark matter halo of mass $10^{12} M_\odot$ at $z = 0$. The derivatives are normalized to the present-day Hubble constant. A constant ($\alpha_{\text{CO}} = 0.8$) prescription is used to convert CO luminosity to molecular hydrogen mass.

changes are calculated as the overall change in the gas and progenitor host halo masses taking place over an incremental redshift interval of $d \ln z = 0.01$. The fractions dM_{HI}/dM_h and dM_{H_2}/dM_h are plotted for the most massive progenitor halo at each redshift with respect to the mass of the descendant halo at $z = 0$. The figures show that atomic gas accretion is dominant for $z \gtrsim 1$ at the lowest halo masses, and decreases with increasing halo mass. It is also seen (consistently with Fig. 2) that the consumption of molecular gas is most efficient for Milky-Way sized galaxies, as indicated by the dip in the H_2 accretion for halo masses $M_h \sim 10^{12} M_\odot$ at $z \sim 0$. For more massive galaxies, the molecular gas is largely accreted at high redshifts, reaching about 20 % of the total baryon fraction. This is consistent with observations (e.g., Conselice et al. 2013) and theoretical predictions (e.g., Dekel et al. 2009) of accretion being the major driver of star formation in massive galaxies at $z \sim 1.5 - 3$.

Fig. 4 shows the logarithmic derivatives of the progenitor halo ($dM_h/M_h H_0 dt$, blue dotted curve), atomic ($dM_{\text{HI}}/M_{\text{HI}} H_0 dt$, orange dot-dashed curve), molecular ($dM_{\text{H}_2}/M_{\text{H}_2} H_0 dt$, green solid curve) and stellar ($dM_*/M_* H_0 dt$, red dashed curve) masses with respect to time, in a descendant dark matter halo of mass $10^{12} M_\odot$ at $z = 0$. The values are normalized to the present-day Hubble constant H_0 . The figure serves to further illustrate the relative contribution of mergers and smooth accretion as a function of redshift. The behaviour indicates that the stellar build-up follows the molecular gas at early times (where the green solid and red dashed curves are close to one another), but becomes merger-dominated at late times, following the halo mass evolution (where the red dashed curve approaches the blue dotted one). This is consistent with the simulations of L’Huillier et al. (2012) and the observational evidences collected by Sánchez Almeida et al. (2014), both of which indicate that smooth accretion, rather than mergers, is the dominant growth mode for gas mass assembly in the majority of high-redshift galaxies ($z > 0.4$), whereas massive galaxies at lower redshifts are primarily merger-dominated. The trends found in the present work are

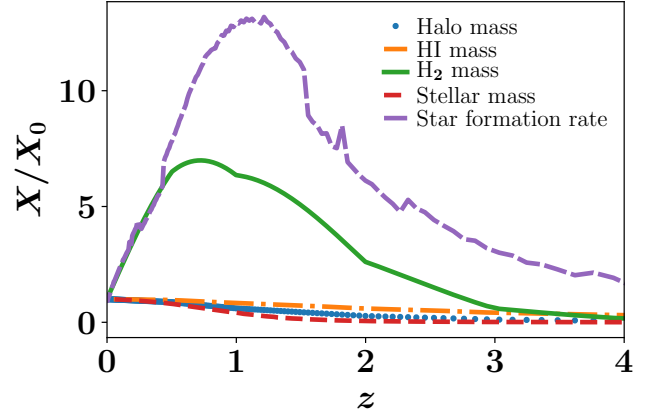


Figure 5. Ratios of the progenitor halo mass (M_h , blue dotted curve), atomic HI mass (M_{HI} , orange dot-dashed curve), molecular H_2 mass (M_{H_2} , green solid curve), stellar mass (M_* , red dashed curve) and star formation rate (purple long-dashed curve) at different redshifts to their present-day values, in a fiducial descendant dark matter halo of mass $M_h = 10^{12} M_\odot$ at $z = 0$. A constant ($\alpha_{\text{CO}} = 0.8$) prescription is used to convert CO luminosity to molecular hydrogen mass.

consistent with the average mass accretion rate into haloes found by Dekel et al. (2013, also discussed in Lilly et al. (2013); Davé et al. (2013)) which are expected to hold for the baryonic accretion as well.

3.4 Star formation and depletion timescale

Finally, we explore the connection between the empirically constrained star formation history (Behroozi et al. 2013c), to the build-up of the various components (atomic, molecular, stellar and progenitor halo masses). The ratios of each of these quantities: the progenitor halo mass (M_h , blue dotted curve), HI mass (M_{HI} , orange dot-dashed curve), H_2 mass (M_{H_2} , green solid curve), stellar mass (M_* , red dashed curve) and star formation rate (SFR, purple long-dashed curve) to their present-day values, are plotted in Fig. 5 as a function of redshift for a fiducial descendant halo of mass $10^{12} M_\odot$ at $z = 0$. The figure indicates that the H_2 mass (not the atomic HI mass) closely traces the star formation rate as a function of cosmic time, with the peak of the SFR build-up occurring slightly earlier than that of the H_2 fraction relative to the present. This is consistent with observational findings that most star formation traces cold, dense gas and molecular clouds rather than warm atomic gas (e.g., Solomon et al. 1987; Bolatto et al. 2008; Bigiel et al. 2008; Leroy et al. 2008), as well as the predictions of the *equilibrium growth/gas regulator models* developed in several theoretical studies (e.g., Bouché et al. 2010; Lilly et al. 2013; Dekel & Mandelker 2014; Peng & Maiolino 2014).

The connection between star formation and molecular gas consumption can be well-quantified by the *depletion time*, which is usually defined as the characteristic timescale for converting molecular gas into stars (e.g., Bigiel et al. 2008; Daddi et al. 2010b; Genzel et al. 2010; Saintonge et al. 2011a; Tacconi et al. 2018; Freundlich et al. 2019). In Figure 6, we plot the mean depletion timescale (computed as $t_{\text{dep}} = M_{\text{H}_2}/\text{SFR}$) as a function of the stellar mass at different redshifts, compared to the results of observations. Solid color linestyles show the results from the present work, and dashed color linestyles show those obtained from the

PHIBSS survey (Tacconi et al. 2018). In both sets, the different colors and marker symbols correspond to the different redshifts: $z = 0$ (blue dots), $z = 1$ (green diamonds), $z = 2$ (red upward triangles), $z = 3$ (yellow downward triangles), and $z = 4$ (purple squares). The black dot-dashed line shows the fitting function derived by Saintonge et al. (2011b) at $z \sim 0$, which is based on observations of $M_* > 10^{10} M_\odot$ galaxies, with its uncertainty range shown by the grey band.

The PHIBSS results find that the depletion timescale for galaxies along the star forming main sequence is well parametrized by a linear trend between $\log t_{\text{dep}}$ and $\log M_*$, with $t_{\text{dep}} \propto \delta M_*^{0.09 \pm 0.05}$ where $\delta M_* = (M_*/5 \times 10^{10} M_\odot)$. The observed weak dependence on the stellar mass is similar to the trend found in our present results. The PHIBSS observations also find a very shallow dependence with redshift, $t_{\text{dep}} \propto (1+z)^{-0.62 \pm 0.13}$, indicating evidence for similar physical processes driving star formation at low and high redshifts. The characteristic value of the depletion timescale found here, $t_{\text{dep}} \sim 1$ Gyr, is also consistent with several other observational results (e.g., Bigiel et al. 2008; Daddi et al. 2010b; Genzel et al. 2010; Tacconi et al. 2013), and earlier semi-empirical work (Popping et al. 2015) that suggest an almost universal depletion timescale across redshifts. At low galaxy masses, we find a somewhat different trend in the depletion timescale compared to the observations (which suggest a decreasing t_{dep} between $z \sim 0 - 2$). This could indicate evidence a lower value of α_{CO} at higher redshifts compared to the present (Bolatto et al. 2013), and/or the impact of UV photodissociation in the low-metallicity ISM which can change the α_{CO} at low galaxy masses (Leroy et al. 2013).

We also note that the presently adopted value of $\alpha_{\text{CO}} = 0.8 M_\odot / (\text{K km/s pc}^2)$ is usually used for mergers, massive starbursts and particularly luminous galaxies above the main sequence. The observational results, on the other hand, use more complicated conversion factors which depend on metallicity (cf. Equation 2-4 of Tacconi et al. (2018), with the metallicity given by Pettini & Pagel (2004)), and thus implicitly depend on stellar mass and redshift through the evolution of an assumed mass-metallicity relation (e.g., Genzel et al. (2015)). Given the uncertainties in these relations and the existence of other factors influencing the resultant α_{CO} (as also noted previously in footnote 3, Sec. 2), we have neglected any differences between the α_{CO} used in the observations and that used in the present analysis (which does not account for changes in α_{CO} with mass and redshift). We note that using a Galactic $\alpha_{\text{CO}} = 4.36 M_\odot / (\text{K km/s pc}^2)$ corrected for mass and metallicity, as advocated by the observations of Tacconi et al. (2018); Freundlich et al. (2019) would increase the tension with the observations, though this could have different possible causes. The conversion factor could indeed be overestimated, but the discrepancy could also be related to the representativity of the different samples used: those implied in the abundance matching relations, and those used by the Saintonge et al. (2011a); Freundlich et al. (2019) and Tacconi et al. (2018) studies – which focus on galaxies on and around the main sequence, which are actively star forming and hence have much larger H_2 content. As such, the depletion times observed in these samples would be lower than in samples that also include quiescent galaxies. Given these considerations, we emphasize that Fig. 6 should be interpreted only as indicative of the average depletion timescales and their trends in evolution with mass and redshift. A detailed study of the variables influencing the CO-to- H_2 conversion factor across redshifts requires inputs from hydrodynamical simulations, and is left to future work.

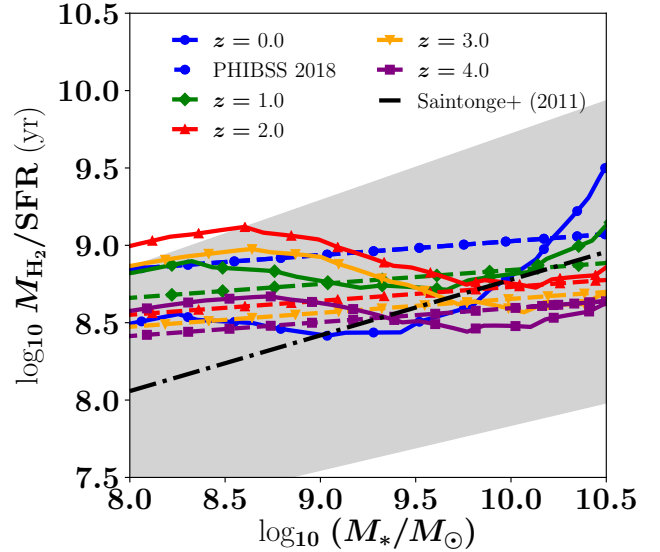


Figure 6. Molecular gas depletion timescale, quantified by the ratio of H_2 mass to star formation rate, as a function of stellar mass at different redshifts. Solid linestyles show the results from the present work, and dashed linestyles show those obtained from the PHIBSS survey (Tacconi et al. 2018). In both sets, the different colors and marker symbols correspond to the different redshifts: $z = 0$ (blue dots), $z = 1$ (green diamonds), $z = 2$ (red upward triangles), $z = 3$ (yellow downward triangles), and $z = 4$ (purple squares). The fitting function derived by Saintonge et al. (2011b) at $z \sim 0$ (which is based on observations of $M_* > 10^{10} M_\odot$ galaxies) is plotted as the dot-dashed line, with its uncertainty range shown by the grey band. A constant $\alpha_{\text{CO}} = 0.8$ is assumed when converting CO luminosity to H_2 mass.

4 SUMMARY AND DISCUSSION

We have developed several data-driven constraints on the build-up of atomic and molecular gas in galactic haloes, and their connections to observed stellar properties. This work brings together existing empirical constraints on the HI mass - halo mass relation and its evolution across redshifts (Padmanabhan & Kulkarni 2017; Padmanabhan et al. 2017), the luminosity and associated halo masses of CO-emitting galaxies across $z \sim 0 - 4$ (Padmanabhan 2018) to calculate molecular gas mass evolution, and the observationally motivated stellar - halo mass (Behroozi et al. 2019) and star formation rate across the same epochs calibrated by Behroozi et al. (2013c). We find the following main results:

(i) The mean stellar/HI mass ratio is almost universal with redshift. The dependence of this ratio with stellar mass is consistent with most observations (including, e.g., the latest findings from Janowiecki et al. 2020, at $z \sim 0$), and indicates that the underlying physics may be independent of redshift and only depend on halo mass. This points to mergers as a possible mode of stellar and atomic gas build-up, which is consistent with the predictions of theoretical models at low redshifts for massive galaxies (e.g., Dekel et al. 2009).

(ii) At high redshifts, we find that most of the star formation is due to smooth accretion, rather than mergers, in Milky-Way sized haloes (of masses $10^{12} M_\odot$ at $z = 0$). This supports the ‘cold mode’ of gas accretion at high redshifts predicted by theoretical models (e.g., Dekel et al. 2009), and implies that most of the star formation is expected to take place in quiescent disk galaxies (e.g.,

Daddi et al. 2010b), rather than merger-driven starbursts at these epochs. It is also, in turn, consistent with the picture of extended galactic disks based on rest-frame UV/optical (e.g., Bell et al. 2005; Elbaz et al. 2007) and H α spectroscopy of galaxies (e.g., Genzel et al. 2008) and Damped-Lyman Alpha (DLA) system observations (e.g., Wolfe et al. 1986) at $z \gtrsim 2$.

(iii) The star formation is strongly connected to the molecular gas (H $_2$) depletion timescale and negligibly to the atomic gas (HI). This reiterates the result, found in several theoretical and observational studies (e.g., Solomon et al. 1987; Bolatto et al. 2008; Bigiel et al. 2008; Leroy et al. 2008; Bouché et al. 2010; Lilly et al. 2013; Dekel & Mandelker 2014; Peng & Maiolino 2014) as well as, e.g. the latest findings of Wang et al. (2020) advocating the role of HI only as an ‘intermediary’ in the process of star formation. It is also consistent with the arguments of Prochaska & Wolfe (2009) that point to a ‘self-correcting balance’ in atomic gas: the HI replenishment from the intergalactic medium is compensated by its conversion to H $_2$ which is consumed by star formation. This, in turn, is linked to the observed constancy of Ω_{HI} , the HI density parameter across redshifts as measured from DLA studies and 21 cm experiments (for a compilation of recent observations, see Padmanabhan et al. (2015) and references therein). Closed box models for gas consumption (e.g., Bauermeister et al. 2010), also advocate the intermediary role of HI in star formation, as coming from ionized gas in the IGM which is ultimately converted into H $_2$.

(iv) The depletion timescale for the consumption of molecular gas, quantified by $t_{\text{dep}} = (M_{\text{H}_2}/\text{SFR})$ is of the order of 0.1 - 1 Gyr, consistently with several observational results (e.g., Kennicutt 1983; Genzel et al. 2010; Tacconi et al. 2018; Freundlich et al. 2019) at $z \sim 0 - 2$. The t_{dep} does not depend strongly on stellar mass, which is also consistent with recent observations (e.g., Janowiecki et al. 2020; Tacconi et al. 2018; Freundlich et al. 2019) at low redshifts. The trend is predicted to hold at higher redshifts as well, suggesting a universality in the Kennicutt-Schmidt relation (Kennicutt 1998). Taken together with the observations of Daddi et al. (2010a); Tacconi et al. (2013) and Genzel et al. (2010), our findings may provide evidence for a decreasing CO-to-H $_2$ conversion factor at high redshifts as compared to its current value.

The key element in this work is the combination of abundance matching empirical relations for the atomic, molecular and stellar mass as a function of halo mass. However, these different components are not independent of each other. A useful way of quantifying the resulting uncertainty is to analyse the accuracy of the abundance matching hierarchy assumed for each component (stars, atomic gas, molecular gas) from the scatter in the respective relations. The typical uncertainties on the gas - halo relations are of the order of a few - 10% at present (depending on redshift, the scatter on the halo model parameters are summarized in Table 3 of Padmanabhan et al. (2017) and Table 1 of Padmanabhan (2018)). For the stellar component, the typical scatter in the SHM may be about 10-20% as illustrated in Behroozi et al. (2010) for Milky-Way sized haloes. The small scatter in the relations does not, however, imply they are independent; we also note that phenomena such as outflows resulting from feedback may invert the hierarchy assumed by the abundance matching technique (for example when depleting the gas).

The empirical constraints developed here serve as an important benchmark for calibrating the results of future simulations and semi-analytical models of galaxy formation that attempt to model the gas and stellar components in a self-consistent manner. In future work, these techniques could be extended to the evolution of

galaxy and HI disc sizes by combining the observations of stellar disks in, e.g., van der Wel et al. (2014) and the empirical evolution of the HI profile derived from Padmanabhan et al. (2017) across redshifts, and exploring the consequences for star formation and ISM physics. Similar results can also be derived for various other dependent relations, including those exploring trends relative to the star-forming main sequence (e.g., Tacconi et al. 2018). Forthcoming observations of atomic (e.g. with the SKA⁴ and its precursors) and molecular gas (e.g. with the ALMA⁵/VLA⁶), as well as gravitational lensing surveys detecting cosmic shear, will be useful to further constrain the physical processes involved to provide a complete picture of galaxy evolution.

ACKNOWLEDGEMENTS

HP thanks Dongwoo Chung and Mubdi Rahman for useful clarifications related to the empirical studies of stellar properties in dark matter haloes. The work of AL was supported in part by the Black Hole Initiative at Harvard University, which is funded by grants from JTF and GBMF. We thank the referee for a detailed and comprehensive report that significantly improved the content and quality of the presentation.

REFERENCES

- Bauermeister A., Blitz L., Ma C.-P., 2010, *ApJ*, **717**, 323
- Behroozi P. S., Conroy C., Wechsler R. H., 2010, *ApJ*, **717**, 379
- Behroozi P. S., Wechsler R. H., Wu H.-Y., 2013a, *ApJ*, **762**, 109
- Behroozi P. S., Wechsler R. H., Wu H.-Y., Busha M. T., Klypin A. A., Primack J. R., 2013b, *ApJ*, **763**, 18
- Behroozi P. S., Wechsler R. H., Conroy C., 2013c, *ApJ*, **770**, 57
- Behroozi P., Wechsler R. H., Hearin A. P., Conroy C., 2019, *MNRAS*, **488**, 3143
- Bell E. F., et al., 2005, *ApJ*, **625**, 23
- Benson A. J., 2012, *New Astron.*, **17**, 175
- Bigiel F., Leroy A., Walter F., Brinks E., de Blok W. J. G., Madore B., Thornley M. D., 2008, *AJ*, **136**, 2846
- Bolatto A. D., Leroy A. K., Rosolowsky E., Walter F., Blitz L., 2008, *ApJ*, **686**, 948
- Bolatto A. D., Wolfire M., Leroy A. K., 2013, *ARA&A*, **51**, 207
- Bouché N., et al., 2010, *ApJ*, **718**, 1001
- Braun R., 2012, *ApJ*, **749**, 87
- Carleton T., et al., 2017, *MNRAS*, **467**, 4886
- Catinella B., et al., 2010, *MNRAS*, **403**, 683
- Catinella B., et al., 2012, *A&A*, **544**, A66
- Catinella B., et al., 2013, *MNRAS*, **436**, 34
- Conselice C. J., Mortlock A., Bluck A. F. L., Grützbauch R., Duncan K., 2013, *MNRAS*, **430**, 1051
- Cortese L., Catinella B., Janowiecki S., 2017, *ApJ*, **848**, L7
- Daddi E., et al., 2010a, *ApJ*, **713**, 686
- Daddi E., et al., 2010b, *ApJ*, **714**, L118
- Davé R., Katz N., Oppenheimer B. D., Kollmeier J. A., Weinberg D. H., 2013, *MNRAS*, **434**, 2645
- Dekel A., Mandelker N., 2014, *MNRAS*, **444**, 2071
- Dekel A., et al., 2009, *Nature*, **457**, 451
- Dekel A., Zolotov A., Tweed D., Cacciato M., Ceverino D., Primack J. R., 2013, *MNRAS*, **435**, 999
- Elbaz D., et al., 2007, *A&A*, **468**, 33
- Font-Ribera A., et al., 2012, *J. Cosmology Astropart. Phys.*, **11**, 59

⁴ <https://www.skatelescope.org/>

⁵ <https://almascience.nrao.edu/about-alm/alm-basics>

⁶ <https://science.nrao.edu/facilities/vla/>

- Freundlich J., et al., 2019, *A&A*, **622**, A105
- Genzel R., et al., 2008, *ApJ*, **687**, 59
- Genzel R., et al., 2010, *MNRAS*, **407**, 2091
- Genzel R., et al., 2015, *ApJ*, **800**, 20
- Girelli G., Pozzetti L., Bolzonella M., Giocoli C., Marulli F., Baldi M., 2020, arXiv e-prints, p. [arXiv:2001.02230](#)
- Guo Q., White S., Li C., Boylan-Kolchin M., 2010, *MNRAS*, **404**, 1111
- Janowiecki S., Catinella B., Cortese L., Saintonge A., Wang J., 2020, arXiv e-prints, p. [arXiv:2001.06614](#)
- Keating G. K., Marrone D. P., Bower G. C., Leitch E., Carlstrom J. E., DeBoer D. R., 2016, *ApJ*, **830**, 34
- Kennicutt R. C. J., 1983, *ApJ*, **272**, 54
- Kennicutt Jr. R. C., 1998, *ApJ*, **498**, 541
- Keres D., Yun M. S., Young J. S., 2003, *ApJ*, **582**, 659
- Kereš D., Katz N., Weinberg D. H., Davé R., 2005, *MNRAS*, **363**, 2
- Klypin A. A., Trujillo-Gomez S., Primack J., 2011, *ApJ*, **740**, 102
- L’Huillier B., Combes F., Semelin B., 2012, *A&A*, **544**, A68
- Leroy A. K., Walter F., Brinks E., Bigiel F., de Blok W. J. G., Madore B., Thornley M. D., 2008, *AJ*, **136**, 2782
- Leroy A. K., et al., 2009, *AJ*, **137**, 4670
- Leroy A. K., et al., 2013, *AJ*, **146**, 19
- Lilly S. J., Carollo C. M., Pipino A., Renzini A., Peng Y., 2013, *ApJ*, **772**, 119
- Martin A. M., Papastergis E., Giovanelli R., Haynes M. P., Springob C. M., Stierwalt S., 2010, *ApJ*, **723**, 1359
- Martin A. M., Giovanelli R., Haynes M. P., Guzzo L., 2012, *ApJ*, **750**, 38
- Moster B. P., Naab T., White S. D. M., 2013, *MNRAS*, **428**, 3121
- Naab T., Ostriker J. P., 2017, *Annual Review of Astronomy and Astrophysics*, **55**, 59
- Nelson D., Vogelsberger M., Genel S., Sijacki D., Kereš D., Springel V., Hernquist L., 2013, *MNRAS*, **429**, 3353
- Noterdaeme P., et al., 2012, *A&A*, **547**, L1
- Padmanabhan H., 2018, *MNRAS*, **475**, 1477
- Padmanabhan H., Kulkarni G., 2017, *MNRAS*, **470**, 340
- Padmanabhan H., Choudhury T. R., Refregier A., 2015, *MNRAS*, **447**, 3745
- Padmanabhan H., Refregier A., Amara A., 2017, *MNRAS*, **469**, 2323
- Peng Y.-j., Maiolino R., 2014, *MNRAS*, **443**, 3643
- Pettini M., Pagel B. E. J., 2004, *MNRAS*, **348**, L59
- Popping G., Somerville R. S., Trager S. C., 2014, *Monthly Notices of the Royal Astronomical Society*, **442**, 2398–2418
- Popping G., Behroozi P. S., Peebles M. S., 2015, *MNRAS*, **449**, 477
- Prochaska J. X., Wolfe A. M., 2009, *ApJ*, **696**, 1543
- Rao S. M., Turnshek D. A., Nestor D. B., 2006, *ApJ*, **636**, 610
- Riebe K., et al., 2011, arXiv e-prints, p. [arXiv:1109.0003](#)
- Rodríguez-Puebla A., Primack J. R., Avila-Reese V., Faber S. M., 2017, *MNRAS*, **470**, 651
- Saintonge A., et al., 2011a, *MNRAS*, **415**, 32
- Saintonge A., et al., 2011b, *MNRAS*, **415**, 61
- Saintonge A., et al., 2017, *ApJS*, **233**, 22
- Sánchez Almeida J., Elmegreen B. G., Muñoz-Tuñón C., Elmegreen D. M., 2014, *The Astronomy and Astrophysics Review*, **22**, 71
- Sheth R. K., Tormen G., 2002, *MNRAS*, **329**, 61
- Solomon P. M., Rivolo A. R., Barrett J., Yahil A., 1987, *ApJ*, **319**, 730
- Somerville R. S., Davé R., 2015, *ARA&A*, **53**, 51
- Somerville R. S., Hopkins P. F., Cox T. J., Robertson B. E., Hernquist L., 2008, *Monthly Notices of the Royal Astronomical Society*, **391**, 481
- Switzer E. R., et al., 2013, *MNRAS*, **434**, L46
- Tacchella S., Bose S., Conroy C., Eisenstein D. J., Johnson B. D., 2018, *ApJ*, **868**, 92
- Tacchella S., et al., 2019, *MNRAS*, **487**, 5416
- Tacconi L. J., et al., 2013, *ApJ*, **768**, 74
- Tacconi L. J., et al., 2018, *ApJ*, **853**, 179
- Walter F., Brinks E., de Blok W. J. G., Bigiel F., Kennicutt Jr. R. C., Thornley M. D., Leroy A., 2008, *AJ*, **136**, 2563
- Wang J., Catinella B., Saintonge A., Pan Z., Serra P., Shao L., 2020, arXiv e-prints, p. [arXiv:2001.01970](#)
- Wolfe A. M., Turnshek D. A., Smith H. E., Cohen R. D., 1986, *ApJS*, **61**, 249
- Zafar T., Péroux C., Popping A., Milliard B., Deharveng J.-M., Frank S., 2013, *A&A*, **556**, A141
- Zwaan M. A., Meyer M. J., Staveley-Smith L., Webster R. L., 2005a, *MNRAS*, **359**, L30
- Zwaan M. A., van der Hulst J. M., Briggs F. H., Verheijen M. A. W., Ryan-Weber E. V., 2005b, *MNRAS*, **364**, 1467
- van der Wel A., et al., 2014, *ApJ*, **788**, 28

This paper has been typeset from a \LaTeX file prepared by the author.